Flux-pumped impedance-engineered broadband Josephson parametric amplifier

J. Grebel,[1] A. Bienfait,[1, a)] É. Dumur,[1, 2, b)] H.-S. Chang,[1] M.-H. Chou,[1, 3] C. R. Conner,[1] G. A. Peairs,[4, 1] R. G. Povey,[1, 3] Y. P. Zhong,[1] and A. N. Cleland[1, 2, c)]

[1)] *Pritzker School of Molecular Engineering, University of Chicago, Chicago IL 60637, USA*

[2)] *Institute for Molecular Engineering and Materials Science Division, Argonne National Laboratory, Lemont IL 60439, USA*

[3)] *Department of Physics, University of Chicago, Chicago IL 60637, USA*

[4)] *Department of Physics, University of California, Santa Barbara CA 93106, USA*

(Dated: 8 March 2021)

Broadband quantum-limited amplifiers serve a critical role in the single-shot readout of superconducting qubits, but a popular implementation, the traveling wave parametric amplifier (TWPA), involves a complex design and fabrication process. Here, we present a simple design for a Josephson parametric amplifier, using a lumped element resonator comprising a superconducting quantum interference device (SQUID) whose useful bandwidth is enhanced with an on-chip impedance-matching circuit. We demonstrate a flux-coupling geometry that maximizes the coupling to the Josephson loop and minimizes spurious excitation of the amplifier resonant circuit. The amplifier, which operates in a flux-pumped mode, is demonstrated with a power gain of more than 20 dB over a bandwidth of about 300 MHz, where approximate noise measurements indicate quantum-limited performance. A procedure is given for optimizing the bandwidth for this kind of amplifier, using a linearized circuit simulation while minimizing non-linearities.

High-fidelity single-shot readout of superconducting qubits requires the lowest-noise amplification to achieve fast discrimination of the intrinsically small readout signals[1–3]. A popular approach is to use traveling wave parametric amplifiers (TWPAs)[4–6], which are broadband low-noise amplifiers approaching quantum-limited performance. Josephson parametric amplifiers (JPAs) provide similar or better noise performance compared to TWPAs[2,7–11] and in addition can operate as phase-sensitive amplifiers. Depending on the implementation, JPAs can also provide tunable operation with bandwidths exceeding 100 MHz with reasonable saturation powers. Here, we explore a number of innovations to improve the performance of a JPA that is simple to fabricate, simple to operate, affords quantum-limited noise amplification over a bandwidth of greater than 300 MHz, and operates in flux-pumped mode, separating the pump from the amplified signal and thereby making post-processing of the signal more straightforward.

The JPA is often viewed as a narrow-band amplifier, because this device is typically designed as a nonlinear resonant cavity whose resonance width determines the useful amplifier bandwidth. TWPAs circumvent this bandwidth limitation by distributing the amplifying nonlinearity over a transmission line[4]. Designs for JPAs that increase the amplification bandwidth while maintaining a simple fabrication process would provide a welcome addition to the Josephson amplifier family[12,13].

A JPA can be designed to amplify signals with either a three-wave or four-wave mixing process, typically implemented using either current-pumping or flux-pumping, respectively[14]. Four-wave JPAs[7] operate with a pump tone ω_p near the signal ω_s and idler ω_i frequencies, with $2\omega_p = \omega_s + \omega_i$ and $\omega_s \approx \omega_i$, where amplification occurs through a fourth-order Kerr non-linearity in the circuit Hamiltonian. Three-wave JPAs[9] operate with a pump tone near twice the signal frequency, $\omega_p = \omega_s + \omega_i$, with amplification due to the frequency modulation of a Josephson superconducting quantum interference device (SQUID) loop. The separation of the pump and signal tones removes the need for post-amplifier filtering circuitry[3]. Flux-pumping with three-wave mixing can be performed with a pump line separated from the signal line, displacing the pump tone from the signal tone both physically and in frequency.

The achievable bandwidth for both four- and three-wave JPAs can be increased significantly, from tens of MHz in a basic design, to hundreds of MHz by impedance-matching the amplifier to its input. This can be achieved by using an impedance-matching taper[15], or, in a particularly simple version of this concept, using a series-connected $\lambda/4$ and $\lambda/2$ impedance transformer[13]. In the latter demonstration, the transformer was off-chip and the JPA was operated in four-wave mode.

Here we extend the work of Ref. 13 using an on-chip impedance transformer and an improved flux coupling to the SQUID that enables flux pumping and both three- and four-wave amplification, with the entire device fabri-

[a)] Present address: Université de Lyon, ENS de Lyon, Université Claude Bernard, CNRS, Laboratoire de Physique, F-69342 Lyon France

[b)] Present address: Université Grenoble Alpes, CEA, INAC-Pheliqs,QuantECA, 38000 Grenoble France

[c)] Electronic mail: anc@uchicago.edu

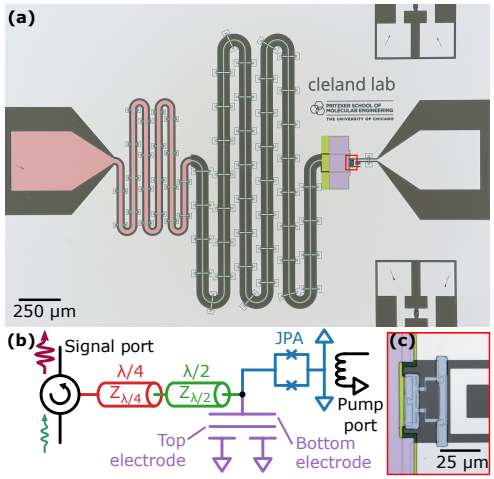

FIG. 1. **Experimental device.** **(a)** Micrograph of fabricated device with a series $\lambda/4$ transformer with impedance $Z_{\lambda/4} = 45\,\Omega$ (red), a $\lambda/2$ transformer with impedance $Z_{\lambda/2} = 80\,\Omega$ (green), and a via-free parallel plate capacitor (purple). **(b)** Circuit representation of device. **(c)** Higher-magnification micrograph of the JPA SQUID (blue) and its associated flux line.

cated monolithically on a single die. The amplifier is operated in reflection, with the input signal reflected as an amplified output signal with a gain of more than 20 dB. This provides a simple design easily integrated with superconducting qubit circuitry. A galvanic connection to the input reduces the coupling quality factor, increasing the amplification bandwidth. A SQUID loop is formed with two Josephson junctions in parallel[16], which when combined with an on-chip flux line, affords *in situ* tuning of the amplifier frequency as well as flux pumping. We use a symmetrically-coupled on-chip flux line that minimizes spurious mode coupling, and thereby enabling operation in a flux-pumped mode. We also use a via-free parallel plate capacitor design with a low-loss dielectric that provides an easily-fabricated pF-range input capacitance. Numerical simulations are used to select device parameters that optimize the amplification bandwidth and minimize non-linearities.

Figure 1 shows images of an impedance-engineered JPA device and its equivalent circuit, fabricated on intrinsic ($> 10\,\mathrm{k\Omega-cm}$ resistivity) silicon. The base wiring is etched from a uniformly-evaporated film of 100 nm thick Al, patterned with a photoresist-masked Cl_2 reactive ion etch process. A $\lambda/4$ resonator centered at 5.3 GHz with characteristic impedance $45\,\Omega$ matches the $50\,\Omega$ impedance input line to $40\,\Omega$, lowering the quality factor of the JPA resonance; the $\lambda/2$ resonator with characteristic impedance $80\,\Omega$, also centered at 5.3 GHz, reduces the frequency dependence in the system susceptibility matrix, thereby increasing the amplification bandwidth[13]. To prevent microwave-frequency slot modes, Al cross-overs with the same dielectric as the capacitor are placed on the impedance-matching resonators every 200 μm[17].

The input to the JPA itself includes a via-free parallel-plate capacitor with total input capacitance $C = 2.03 \pm 0.02\,\mathrm{pF}$ to ground. The impedance-transformed input line is galvanically connected to the bottom capacitor plate, which is in turn galvanically connected to the SQUID. The capacitor top electrode is formed by a 200 nm thick Al film on a 250 nm thick dielectric, the dielectric formed by 10 nm thick silicon nitride (SiN) layers on the top and bottom for improved film quality, with the remaining thickness comprising hydrogen-saturated amorphous silicon (*a*-Si), chosen for its low dielectric loss[18]. The top capacitor plate is capacitively coupled to ground, in parallel with the SQUID, and has no galvanic connections. The SQUID is formed by two identical Josephson junctions connected in parallel, designed to have a combined critical current of 2.64 μA and an enclosed loop area of $220\,\mu\mathrm{m}^2$. The SQUID and its flux-pumping line, shown in detail in Fig. 1c, are designed to have mirror symmetry about the SQUID connection point to the capacitor base, thereby minimizing the coupling of microwave-frequency pump tones to spurious modes; the flux pumping line also includes a single grounded Al cross-over.

Choosing the JPA parameters is a non-trivial optimization problem: An ideal JPA is designed to maximize its amplification bandwidth and saturation power, while minimizing added noise. Approximate analytic solutions can be used to guide simple device designs[21], however numerical simulations are more appropriate for simultaneously optimizing multiple parameters. We optimized using numerical simulations based on the pumpistor model[19,20], where the SQUID, in the presence of a parametric flux pump, is modeled as a linear inductance combined with an effective negative resistance, as shown in Fig. 2a. We note that this specific model for the SQUID is only valid for the three-wave non-degenerate mode of operation. The impedance-transforming input circuit is modeled using standard transmission-line equations. The SQUID inductances $L_{n,0}$ and $L_{n,2}$ are defined[20] as

$$L_{n,0} = L_J/\epsilon_0, \tag{1}$$

$$L_{n,2} = -\frac{L_J}{|\epsilon_1|^2}\left(\epsilon_0 - j\omega_i L_J Y_i^*\right), \tag{2}$$

where $L_J = L_s/\cos(\pi\Phi_{\mathrm{DC}})$, $\epsilon_0 = 1 - (1/4)(\pi\Phi_{\mathrm{AC}})^2$, and $\epsilon_1 = (\pi\Phi_{\mathrm{AC}}/2)\tan(\pi\Phi_{\mathrm{DC}})$. These parameters are functions of the SQUID bare inductance L_s, the DC flux Φ_{DC}, the AC flux amplitude Φ_{AC}, and the external admittance Y_i seen by the SQUID at the idler frequency ω_i .

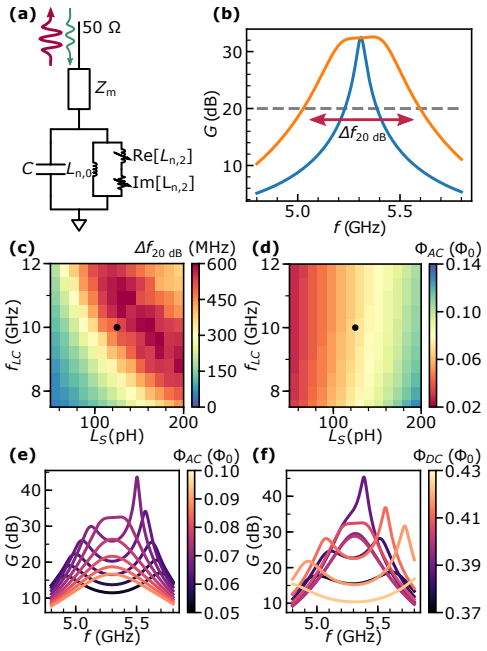

FIG. 2. **JPA simulated power gain and bandwidth using the pumpistor model**[19,20]. **(a)** Linearized circuit used for simulations with impedance-matching element Z_m, JPA capacitance $C = 2.03\,\mathrm{pF}$, SQUID static inductance $L_{\mathrm{n},0}$, SQUID variable inductance $\mathrm{Re}[L_{\mathrm{n},2}]$ and variable resistance (imaginary inductance) $\mathrm{Im}[L_{\mathrm{n},2}]$. The variable circuit elements are functions of the pump amplitude Φ_{AC} and the DC flux Φ_{DC}, plotted in units of the flux quantum $\Phi_0 = h/2e$ in panels d, e and f. **(b)** Simulated power gain curve $G(f)$ as a function of signal frequency f for a JPA circuit with (orange) and without (blue) the impedance-matching element Z_m. Red arrows indicate the bandwidth $\Delta f_{20\mathrm{dB}}$ for which the power gain is greater than 20 dB. **(c)** Bandwidth $\Delta f_{20\mathrm{dB}}$ and **(d)** Φ_{AC} calculated for the optimized operating point as a function of the bare SQUID inductance L_s and bare LC resonance frequency $f_{LC} = 1/(2\pi\sqrt{L_S C})$. Black dots show design parameters for the fabricated device, where $L_s = 125\,\mathrm{pH}$ and $f_{LC} = 10\,\mathrm{GHz}$. **(e)** Simulated gain curves with $L_s = 125\,\mathrm{pH}$ and $f_{LC} = 10\,\mathrm{GHz}$, for different Φ_{AC} and **(f)** Φ_{DC}, near the operating point where $\Phi_{\mathrm{DC}} = 0.41\,\Phi_0$, and $\Phi_{\mathrm{AC}} = 0.073\,\Phi_0$.

This allows us to model the JPA power gain $G(f)$ as a function of frequency, shown for typical parameters in Fig. 2b, both with and without the input impedance transformer. The transformer significantly increases the bandwidth $\Delta f_{20\mathrm{dB}}$ over which the gain is larger than 20 dB, as shown by the red arrow. We choose a 20 dB bandwidth because, at that gain, the noise contribution from typical cryogenic second-stage amplifiers can be neglected. In our setup, for example, we use a high-electron-mobility transistor (HEMT) amplifier with a noise temperatures of ∼2 K, which referenced to the JPA input is reduced to ∼ 20 mK for a gain of 20 dB[22], contributing a small amount to the quantum-limited noise of $hf/k_B = 240\,\mathrm{mK}$ at $f = 5\,\mathrm{GHz}$.

The response of the JPA depends critically on the SQUID design parameters. In Figs. 2c and d we show the bandwidth $\Delta f_{20\mathrm{dB}}$ (color scale) and the flux pump modulation amplitude Φ_{AC}, calculated as a function of the SQUID linearized inductance L_s and the SQUID bare LC frequency $f_{LC} = 1/(2\pi\sqrt{L_s C})$. These are optimized at each operating frequency by first setting Φ_{DC} to achieve a gain greater than 20 dB with minimal Φ_{AC}, and then varying Φ_{AC} to maximize the bandwidth. When choosing device parameters, one might pick a SQUID inductance L_s to maximize the bandwidth; however, a practical JPA design should also minimize the pump amplitude Φ_{AC} in order to reduce non-linearities in the pumping process. As seen in Figs. 2c and d, these two criteria are in opposition; here we compromise and chose device parameters that optimize the bandwidth while keeping the pump amplitude below $0.1\,\Phi_0$, shown by the black dots in the panels, with $L_s = 125\,\mathrm{pH}$ and $f_{LC} = 10\,\mathrm{GHz}$.

With fixed physical parameters L_s and f_{LC}, the gain curve $G(f)$ still depends on the flux-bias operating point Φ_{DC} as well as the modulation amplitude Φ_{AC} of the flux pump, as shown in Figs. 2e and f.

The frequency and value of the maximum JPA gain also depend on the detailed input circuit[13,15]. We model the input line as an ideal 50 Ω impedance connected to the input impedance transformers. In a real device, the input would include non-ideal circulators, cables, and wire-bond connections, each modifying the gain-frequency $G(f)$ response. Note that the impedance transformer can be chosen to yield large bandwidths in simulation, but JPA impedances below 10 Ω are difficult to optimally match to a 50 Ω input line impedance and furthermore optimally matching these impedances increases the required flux modulation Φ_{AC}. We chose impedance transformer parameters that are reasonable to fabricate, then optimized the JPA parameters given this fixed input circuit.

The device is operated on the mixing chamber plate of a dilution refrigerator with a base temperature of 7 mK. The signal is measured in reflection and then amplified using a commercial HEMT amplifier. With no AC flux pump, two resonances are visible as the DC flux is varied, shown in Fig. 3a. These resonances match a linear circuit model including the $\lambda/4$ and $\lambda/2$ transmission lines loaded by a parallel lumped-element LC resonator, where the SQUID inductance is modeled by the flux-biased inductance $L_J = L_s/\cos(\pi\Phi_{\mathrm{DC}})$. The model lumped-element capacitance C and inductance L_J are assumed to have their design values, and both impedance-matching transmission line resonator frequencies are taken as 5.3 GHz. After solving numerically for the impedance of this model as a function of frequency,

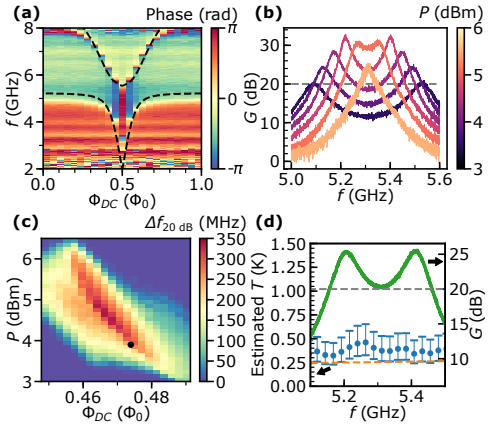

FIG. 3. **Measured device performance, operated in a dilution refrigerator at 7 mK. (a)** Phase of small signal reflected from amplifier as a function of frequency f and DC flux $\Phi_{\rm DC}$. Dashed lines are indicate resonances in a linear circuit model of the device without flux pumping. **(b)** Power gain $G(f)$ as a function of frequency for various signal generator powers P at $\Phi_{\rm DC} = 0.47\,\Phi_0$. **(c)** Bandwidth $\Delta f_{\rm 20dB}$ as a function of pump power P and DC flux $\Phi_{\rm DC}$. **(d)** Measured gain $G(f)$ (green) and estimated noise temperature (blue) versus frequency f at labeled point in panel c, displaying 300 MHz bandwidth. The noise quantum limit (orange) is given by $T_N = hf/k_b$. Noise temperature error bars are dominated by uncertainty in effective HEMT noise temperature.

the resonance is defined[23] as the frequency at which the reactive input impedance is zero.

In Fig. 3b we display the power gain $G(f)$ for various pump powers P (measured at the top of the cryostat), measured with $\Phi_{\rm DC} = 0.47\,\Phi_0$. A pump power of 4 dBm corresponds to $\Phi_{\rm AC} = 0.07\,\Phi_0$, assuming the known cable attenuation of -40 dBm and using the SQUID's estimated DC mutual inductance with the flux line of 1.35 pH; the value of $\Phi_{\rm AC}$ is consistent with simulations. The bandwidth $\Delta f_{\rm 20dB}$ is measured as a function $\Phi_{\rm DC}$ and pump power P for a pump frequency of 10.62 GHz (see Fig. 3b). We choose values of $\Phi_{\rm DC}$ and P that minimize the JPA noise and maximize the bandwidth. Using the optimized parameters, we measure $\Delta f_{\rm 20dB} = 305$ MHz (see Fig. 3d). A 1 dB saturation power of -116 dBm is measured for these operating parameters, which is similar to other lumped-element amplifiers[12].

The noise temperature is roughly estimated using the HEMT as a calibration source (Fig. 3d), by comparing the signal-to-noise ratio for a weak signal while flux-pumping the JPA to that without flux-pumping. The amplification chain includes the JPA, attenuating elements following the JPA, then the cryogenic HEMT amplifier. Circulators, cables, and connections between components are estimated to attenuate the signal between the JPA and HEMT by approximately 2.6 ± 1.5 dB. The noise temperatures for the HEMT and JPA are then calculated by dividing the noise of each element N_i by $k_B B$ where $B = 3$ MHz is the measurement bandwidth. This assumes the JPA has unity gain when off, and that the JPA when on, and the HEMT gain, are both much larger than 1. The estimated JPA noise temperature is consistent with near-quantum-limited operation.

In summary, we have demonstrated a simple impedance-matched Josephson parametric amplifier with an on-chip impedance transforming circuit that we operate in a three-wave (flux-pumped) mixing mode, yielding a simple monolithic device with pump separated from the signal. The amplifier displays a large operating bandwidth of greater than 300 MHz with good noise performance. This device has also been measured in a four-wave (current-pumped) mixing mode with an operating bandwidth of 200 MHz with an average noise of 460 mK over its operating bandwidth. While here we report on a single device, similar performance has been measured in other devices with similar design parameters. The straightforward design and fabrication of this device makes it more accessible to a wider range of researchers who need a robust and simple broadband near-quantum-limited amplifier for microwave measurements.

Data Availability Statement

The data that support the findings of this study are available from the corresponding author upon reasonable request.

Acknowledgements

We thank P. J. Duda for helpful discussions. Devices and experiments were supported by the Army Research Laboratory. É.D. was supported by LDRD funds from Argonne National Laboratory; A.N.C. was supported in part by the DOE, Office of Basic Energy Sciences. This work was partially supported by the UChicago MRSEC (NSF DMR-2011854) and made use of the Pritzker Nanofabrication Facility, which receives support from SHyNE, a node of the National Science Foundation's National Nanotechnology Coordinated Infrastructure (NSF ECCS-2025633). The authors declare no competing financial interests. Correspondence and requests for materials should be addressed to A. N. Cleland (anc@uchicago.edu).

[1] A. A. Clerk, M. H. Devoret, S. M. Girvin, F. Marquardt, and R. J. Schoelkopf, "Introduction to quantum noise, measurement, and amplification," Rev. Mod. Phys. **82**, 1155–1208 (2010).

[2]R. Vijay, D. H. Slichter, and I. Siddiqi, "Observation of quantum jumps in a superconducting artificial atom," Phys. Rev. Lett. **106**, 110502 (2011).
[3]P. Krantz, M. Kjaergaard, F. Yan, T. P. Orlando, S. Gustavsson, and W. D. Oliver, "A quantum engineer's guide to superconducting qubits," Applied Physics Reviews **6**, 021318 (2019), https://doi.org/10.1063/1.5089550.
[4]C. Macklin, K. O'Brien, D. Hover, M. E. Schwartz, V. Bolkhovsky, X. Zhang, W. D. Oliver, and I. Siddiqi, "A near–quantum-limited Josephson traveling-wave parametric amplifier," Science **350**, 307–310 (2015), http://science.sciencemag.org/content/350/6258/307.full.pdf.
[5]T. C. White, J. Y. Mutus, I.-C. Hoi, R. Barends, B. Campbell, Y. Chen, Z. Chen, B. Chiaro, A. Dunsworth, E. Jeffrey, J. Kelly, A. Megrant, C. Neill, P. J. J. O'Malley, P. Roushan, D. Sank, A. Vainsencher, J. Wenner, S. Chaudhuri, J. Gao, and J. M. Martinis, "Traveling wave parametric amplifier with Josephson junctions using minimal resonator phase matching," Applied Physics Letters **106**, 242601 (2015), https://doi.org/10.1063/1.4922348.
[6]L. Planat, A. Ranadive, R. Dassonneville, J. Puertas Martínez, S. Léger, C. Naud, O. Buisson, W. Hasch-Guichard, D. M. Basko, and N. Roch, "Photonic-crystal Josephson traveling-wave parametric amplifier," Phys. Rev. X **10**, 021021 (2020).
[7]B. Yurke, L. R. Corruccini, P. G. Kaminsky, L. W. Rupp, A. D. Smith, A. H. Silver, R. W. Simon, and E. A. Whittaker, "Observation of parametric amplification and deamplification in a Josephson parametric amplifier," Phys. Rev. A **39**, 2519–2533 (1989).
[8]I. Siddiqi, R. Vijay, F. Pierre, C. M. Wilson, M. Metcalfe, C. Rigetti, L. Frunzio, and M. H. Devoret, "Rf-driven Josephson bifurcation amplifier for quantum measurement," Phys. Rev. Lett. **93**, 207002 (2004).
[9]M. A. Castellanos-Beltran and K. W. Lehnert, "Widely tunable parametric amplifier based on a superconducting quantum interference device array resonator," Applied Physics Letters **91**, 083509 (2007), https://doi.org/10.1063/1.2773988.
[10]T. Yamamoto, K. Inomata, M. Watanabe, K. Matsuba, T. Miyazaki, W. D. Oliver, Y. Nakamura, and J. S. Tsai, "Flux-driven Josephson parametric amplifier," Applied Physics Letters **93**, 042510 (2008), https://doi.org/10.1063/1.2964182.
[11]N. Bergeal, F. Schackert, M. Metcalfe, R. Vijay, V. E. Manucharyan, L. Frunzio, D. E. Prober, R. J. Schoelkopf, S. M. Girvin, and M. H. Devoret, "Phase-preserving amplification near the quantum limit with a Josephson ring modulator," Nature **465**, 64–68 (2010).
[12]J. Y. Mutus, T. C. White, E. Jeffrey, D. Sank, R. Barends, J. Bochmann, Y. Chen, Z. Chen, B. Chiaro, A. Dunsworth, J. Kelly, A. Megrant, C. Neill, P. J. J. O'Malley, P. Roushan, A. Vainsencher, J. Wenner, I. Siddiqi, R. Vijay, A. N. Cleland, and J. M. Martinis, "Design and characterization of a lumped element single-ended superconducting microwave parametric amplifier with on-chip flux bias line," Appl. Phys. Lett. **103**, 122602 (2013).
[13]T. Roy, S. Kundu, M. Chand, A. M. Vadiraj, A. Ranadive, N. Nehra, M. P. Patankar, J. Aumentado, A. A. Clerk, and R. Vijay, "Broadband parametric amplification with impedance engineering: Beyond the gain-bandwidth product," Applied Physics Letters **107**, 262601 (2015), https://doi.org/10.1063/1.4939148.
[14]S. Boutin, D. M. Toyli, A. V. Venkatramani, A. W. Eddins, I. Siddiqi, and A. Blais, "Effect of higher-order nonlinearities on amplification and squeezing in Josephson parametric amplifiers," Phys. Rev. Applied **8**, 054030 (2017).
[15]J. Y. Mutus, T. C. White, R. Barends, Y. Chen, Z. Chen, B. Chiaro, A. Dunsworth, E. Jeffrey, J. Kelly, A. Megrant, C. Neill, P. J. J. O'Malley, P. Roushan, D. Sank, A. Vainsencher, J. Wenner, K. M. Sundqvist, A. N. Cleland, and J. M. Martinis, "Strong environmental coupling in a Josephson parametric amplifier," Applied Physics Letters **104**, 263513 (2014), https://doi.org/10.1063/1.4886408.
[16]C. D. Tesche and J. Clarke, "Dc squid - noise and optimization," Journal of Low Temperature Physics **29**, 301–331 (1977).
[17]G. E. Ponchak, J. Papapolymerou, and M. M. Tentzeris, "Excitation of coupled slotline mode in finite-ground CPW with unequal ground-plane widths," IEEE Transactions on Microwave Theory and Techniques **53**, 713–717 (2005).
[18]A. D. O'Connell, M. Ansmann, R. C. Bialczak, M. Hofheinz, N. Katz, E. Lucero, C. McKenney, M. Neeley, H. Wang, E. M. Weig, A. N. Cleland, and J. M. Martinis, "Microwave dielectric loss at single photon energies and millikelvin temperatures," Applied Physics Letters **92**, 112903 (2008), https://doi.org/10.1063/1.2898887.
[19]K. M. Sundqvist, S. Kintaş, M. Simoen, P. Krantz, M. Sandberg, C. M. Wilson, and P. Delsing, "The pumpistor: A linearized model of a flux-pumped superconducting quantum interference device for use as a negative-resistance parametric amplifier," Applied Physics Letters **103**, 102603 (2013), https://doi.org/10.1063/1.4819881.
[20]K. M. Sundqvist and P. Delsing, "Negative-resistance models for parametrically flux-pumped superconducting quantum interference devices," EPJ Quantum Technology **1**, 6 (2014).
[21]C. Eichler and A. Wallraff, "Controlling the dynamic range of a Josephson parametric amplifier," EPJ Quantum Technology **1**, 2 (2014).
[22]H. T. Friis, "Noise figures of radio receivers," Proceedings of the IRE **32**, 419–422 (1944).
[23]S. E. Nigg, H. Paik, B. Vlastakis, G. Kirchmair, S. Shankar, L. Frunzio, M. H. Devoret, R. J. Schoelkopf, and S. M. Girvin, "Black-box superconducting circuit quantization," Phys. Rev. Lett. **108**, 240502 (2012).